

**Methods and outcomes of the COMRADE project -
Design of robust Combined control for robotic spacecraft and manipulator in servicing missions:
comparison between between Hinf and nonlinear Lyapunov-based approaches**

**Pablo Colmenarejo^{a*}, Joao Branco^b, Nuno Santos^b, Pedro Serra^{bi}, Juergen Telaar^c, Hans Strauch^c,
Michael Fruhnert^c, Alessandro M. Giordano^{id}, Marco De Stefano^d, Christian Ott^d, Matthias Reiner^d, David
Henry^e, Jaroslaw Jaworski^f, Evangelos Papadopoulos^g, Gianfranco Visentin^h, Finn Ankersen^h, Jesus Gil-
Fernandez^h**

^a GMV, Isaac Newton 11, P.T.M. Tres Cantos, E-28760 Madrid, Spain, pcolmena@gmv.com

^b GMV Skysoft, Av. D. João II, n° 43, Torre Fernão de Magalhães 7º, 1998-025 Lisboa, Portugal,
jbranco@gmv.com, nuno.santos@gmv.com, parroz@gmv.com

^c Airbus Defence and Space, Airbus Allee 1, 28199 Bremen, Germany, juergen.telaar@airbus.com,
hans.strauch@airbus.com, michael.fruhnert.external@airbus.com

^d Deutsches Zentrum für Luft- und Raumfahrt (DLR e.V.), Institute of Robotics and Mechatronics, 82234, Wessling,
Germany, Alessandro.Giordano@dlr.de, Marco.DeStefano@dlr.de, Christian.Ott@dlr.de, Matthias.Reiner@dlr.de

^e Bordeaux University - IMS-LAPS, 351 Cours de la Libération, 33405 Talence, France, david.henry@u-bordeaux.fr

^f Przemysłowy Instytut Automatyki i Pomiarów (PIAP), Jerozolimskie 202, 02-486 Warsaw, Poland,
jaroslaw.jaworski@piap-space.com

^g NTUA, 9 Heroon Polytechniou, GR- 15780 Zografou, Athens, Greece, egpapado@central.ntua.gr

^h ESA/ESTEC, Keplerlaan 1, 2201 AZ Noordwijk, Netherlands, Gianfranco.Visentin@esa.int,
Finn.Ankersen@esa.int, jesus.gil.fernandez@esa.int

ⁱ Department of Informatics, Technical University of Munich, Garching, Germany

^j Lusofona University of Humanities and Technologies ULHT / ECATI / COPELABS, Lisbon, Portugal

* Corresponding Author

Abstract

Extending life or repairing damaged on-orbit assets is not only a very attractive economic option for satellite operators as it could potentially increase margins for commercial services or increasing delivered value of scientific missions, but it would also help reducing the number of debris objects in space.

These types of servicing missions pose technical challenges never faced until now. Of utmost relevance is the autonomous control of several movable devices, whose dynamics are inter-coupled (e.g., spacecraft platform, robotic manipulator, and end-effector), needed to safely and effectively achieve the mission objective.

In the frame of ESA-supported COMRADE study, fully combined control (single control system controlling simultaneously all movable devices) is proposed due to its higher improvement potential (propellant saving, performances increase, safety) w.r.t. tele-operation, decoupled and/or collaborative control (the last one characterized by the use of two different control systems for the spacecraft platform and robotic manipulator respectively but, differently to the decoupled version, with information/feedback about what the other control system intends to do). Two independent combined control designs are developed in COMRADE (H_∞ and nonlinear Lyapunov-based), and tested. Each of them is applied for both Active Debris Removal (ADR) and servicing/re-fuelling mission scenarios. This paper presents: the processes of scenario analysis and derivation of COMRADE system requirements; a description of the design and setup for a Simulator, which included at its core the selection, prototyping and integration of algorithms for Guidance, Navigation and Control (GNC), Modes Management (AMM) and Failures Detection, Isolation and Recovery (FDIR) (all three together compose the COMRADE system) and the outcomes of the simulation phase of the Verification & Validation process.

Keywords: robotic, servicing, debris removal, robust control, compliant control, Envisat

Acronyms/Abbreviations

AOCS	Attitude and Orbit Control System	CoM	Center of Mass
APE	Absolute Pointing Error	COMRADE	Chaser Control Systems Design, Analysis and Trade-off
ASSIST	hArmonised System Study on Interfaces and Standardisation of fuel Transfer	DDVV	Design Development Validation and Verification
CAM	Collision Avoidance Manoeuvre	DKE	Dynamics, Kinematics, Environment
		DOF	Degree of Freedom

ESA	European Space Agency
FDA	Failure Detection and Accomodation
FDI	Failure Detection and Isolation
FES	Functional Engineering Simulator
FOV	Field of View
FTC	Failure Tolerant Control
GEO	Geosynchronous Earth Orbit
GNC	Guidance, Navigation, and Control
GNCDE	GNC Development Environment
GPS	Global Positioning System
HIL	HW-In-the-Loop
HW	Hardware
I/O	Input/Output
IMU	Inertial Measurement Unit
LAR	Launcher Adapter Ring
LFT	Linear Fractionated Transfer function
LIDAR	Light Detection and Ranging (system)
LVLH	Local Vertical Local Horizontal
MCI	Mass, Centrum and Inertia
MIL	Model-In-the-Loop
MIMO	Multiple Input Multiple Output
N/A	Not Applicable
PD	Proportional Derivative (control)
RdV	RendezVous
SC	Spacecraft
SK	Station Keeping
SW	Software
TGFF	Target Geometry Fixed Frame
TITOP	Two Input Two Output Port
TRL	Technology Readiness Level
UIO	Unknown Input Observer
ΔV	delta V

1. Introduction

The current space debris environment poses a safety hazard to operational spacecraft as well as a hazard to public safety and property in cases of uncontrolled re-entry events.

The accidental 2009 satellite collision between Iridium 33 and Cosmos-2251 led to a debris cloud with up to 823 new large debris object catalogued two months later after the collision and many others not catalogued [1]. This was the origin of different studies about the current space debris environment performed by all major space agencies, showing that even if no further space launches took place the space debris population would continue to increase.

While debris mitigation measures are being implemented by ESA and by many other space actors, the studies demonstrate that there is a continuously growing collision risk and something needs to be done to cap debris population increase and hence reduce risk. Among the different possible remediation actions is Active Debris Removal (ADR).

Active removal efficiency is increased when applied to objects with high mass, high collision probabilities and at high altitudes, and applied early enough to prevent the further degradation of the environment. For this reason ESA is pursuing the development of the eDeorbit mission that will remove a large defunct satellite from the Sun synchronous orbit: ENVISAT.

1.1 Technological background

The COMRADE activity pertains only to a particular technological means for ADR that involves a chaser equipped with robot(s) being operated in tight coordination with the chaser platform motion.

In this particular technological context, it is important to observe that historically decoupled control and collaborative control have been investigated to some extent and have shown that solutions based on them seem to work for some simulated cases (e.g. German DEOS mission and ESA e.Deorbit studies targeting ENVISAT satellite). However, concerns are raised by the fact that the attribution of control authority to the robot and platform is arbitrary, tailored to the specific situation and may not be adequate if the actual situation in the ADR mission differs from that modelled ahead of the mission. In addition, the rigid attribution of control authority limits the possibility to treat failures and anomalies with a coordinated approach that may use the highly redundant motion ability of the chaser (possibly higher than 12 degrees of freedom) to continue the operation unaffected by the contingency.

1.2 Objectives

The objective of the activity was to design, develop, and test the control system of a robotic spacecraft (i.e. a servicing spacecraft equipped with a manipulator) tasked to perform an Active Debris Removal and a refuelling mission. This control system, referred to as Chaser Control System, provides for combined control and management of the whole chaser, in the operations of grasping, stabilisation and hold of the debris with the aim to perform the controlled de-orbit.

The Chaser Control System presented herein:

- handles its own internal control modes to perform the tasks and have communication with the higher level Chaser Control System;
- is designed as a multi variable combined control system fulfilling the mission operational constraints and the performance requirements;
- is designed using modern robust multi variable synthesis methods able to handle the uncertainties of the system;
- considers in its implementation technological constraints posed by state of the art equipment and use integrated design methods leading to that;
- achieves high level of Reliability, Availability and Safety of the control software.

2. Missions Description

The study considers two mission scenarios: the e.Deorbit space debris removal mission and the servicing scenario as defined in the ASSIST study.

2.1 ADR/e.deorbit

The e.Deorbit mission objective is to “Remove a single large ESA-owned Space Debris from the LEO protected zone”.

The mission consists of a satellite (Chaser) that is launched by a small or medium launcher (Vega-C), performs a rendezvous with the ESA-owned debris ENVISAT (Target), captures and removes the Target from the LEO protected zone. For both Chaser and Target, the ESA mitigation rules defined in [2] apply. The Chaser shall comply to the MSRD [3].

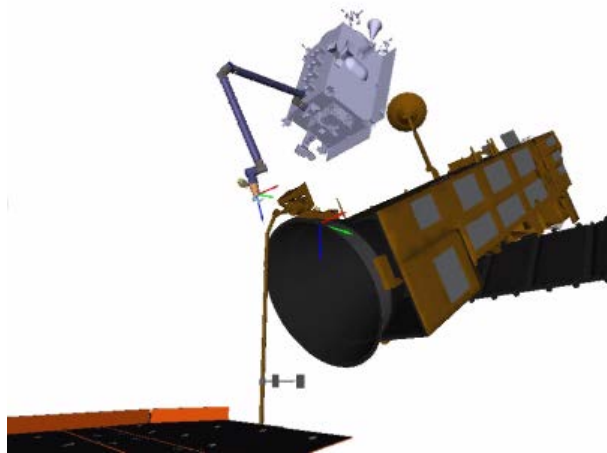


Fig. 1. E.deorbit mission concept at capture phase.

COMRADE is limited to the Synchronisation, Capture, Rigidisation and Stabilisation phases. The Synchronisation starts with a transition from Parking Hold Point to Capture Point. The motion synchronisation strategy comprises several steps:

- V-bar approach from 100 to 30 m (LVLH);
- Spherical Fly-around to Target angular momentum vector (LVLH);
- Approach along angular momentum vector (LVLH);
- Synchronisation of rotational motion (transition to Target reference frame);
- Transfer to Capture Point (Target reference frame).

At the Capture Point the robot arm moves the open gripper to the Grasping Point at the LAR (Fig. 1). As soon as the gripper is in the right position for grasping it closes rapidly establishing a form closure assuring that the LAR cannot escape. Then the gripper closes rigidly establishing a stiff connection between gripper and LAR. After confirmation of successful capture the robot arm is rigidised. The stabilisation of the coupled system of Chaser and Target begins upon confirmation of arm rigidisation.

2.2 Refuelling/ASSIST

As a baseline for the ASSIST mission, a reference scenario was defined at the beginning of the ESA “hArmonised System Study on Interfaces and Standardisation of fuel Transfer (ASSIST)” activity [4]. The ASSIST system shall be compatible with:

- Large GEO telecom satellites (~4-6-8 Tn.)
 - Small GEO telecom satellites (around 1.8-3.5 Tn.)
- COMRADE however focus on the lower inertia configuration for contrasting with the ARD/e.deorbit case. Moreover, a capture probe (Fig. 2, bottom) replaces the gripper mounted on the end-effector of the robot arm, whereas the target accommodates a berthing fixture (Fig. 2, top).

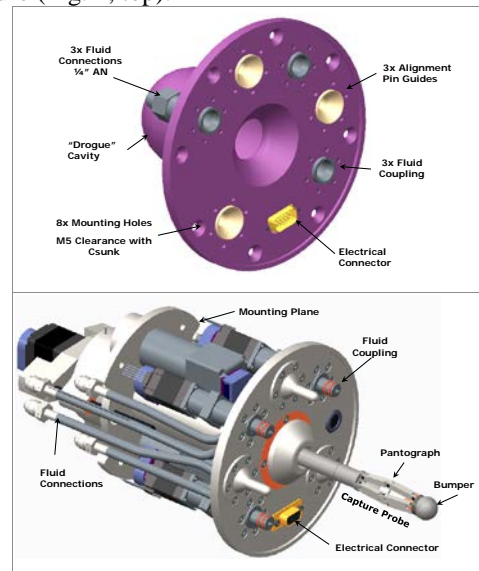


Fig. 2. ASSIST system components.

The proposed on-orbit servicing mission includes the following phases:

- The rendezvous final/terminal phase, which begins when the servicing S/C detects the serviced S/C by its own sensing means and starts the relative navigation phase. COMRADE assumed a relative distance between 100m and a meter range (e.g. 1.25m) (compatible within the maximum reach of the robotic arm mounted on the servicing S/C). During this phase the robotic arm is folded in the servicing S/C body.
- The berthing phase, which is entirely operated by the robotic arm, whose objective is to mate the servicing S/C end-effector part with the serviced S/C berthing fixture counterpart. The robotic arm should be equipped with an illumination source in order to provide a clear view of the markers placed on the berthing fixture mechanism.
- After the end-effector capture probe contacts the drogue cavity of the berthing fixture a central mechanism will be retracted to ensure an initial soft

docking. Later on a second phase of mechanical engagement using aligning pins will be performed ensuring a hard docking (Hard-dock Mode). This phase ends with a successful berthing/mating and subsequent connection of fuel, gas and electrical interfaces.

3. System requirements

The Chaser Control System shall comply with the requirements presented herein. Table 1, Table 2, and Table 3 collect the performance specifications respectively for Synchronisation, Reach, and Stabilisation phases. Table 4 collects the safety specifications.

Table 1. Synchronisation performance requirements.

The Chaser GNC, during the Synchronization Phase, shall be capable of providing the following performance requirements:

- The relative position APE (chaser COM wrt target COM) shall be better than 0.1 m with 95% probability.
- The relative velocity APE (chaser COM wrt target COM) shall be better than 0.01 m/s with 95% probability.

The attitude control error shall be $< 2^\circ$ during Synchronized Flight.

The angular rate control error shall be $< 0.5^\circ/\text{s}$ during Synchronized Flight.

Table 2. Reach phase performance requirements.

The Chaser GNC, during the Capture Phase, shall be capable of providing the performance requirements imposed by the capture mechanism, as a minimum

- Position APE of the COM of the chaser wrt a capture reference point better than 0.05 m with 95% probability. Note: this reference point is defined on TGFF for GNC purposes and it is not necessarily the capture point.
- Velocity APE of the COM of the chaser wrt a capture reference point better than 0.005 m/s with 95% probability.
- Attitude APE of the chaser wrt the desired capture attitude in TGFF better than 2 deg with 95% probability.
- Angular velocity APE of the chaser wrt the desired capture attitude in TGFF better than 0.5 deg/s with 95% probability.

At the time of grappling, the combined control including visual tracking shall keep the robotic arm end-effector within the gripper grappling envelope:

- $x = \pm 10 \text{ mm}$
- $y = \pm 22 \text{ mm}$
- $z = \pm 22 \text{ mm}$
- Pitch = $\pm 2.74 \text{ deg}$
- Yaw = $\pm 2.74 \text{ deg}$
- Roll = $\pm 2.74 \text{ deg}$

The relative velocity control error between gripper and

grasping point shall be below 0.005 m/s for each axis.

The relative angular rate control error between gripper and grasping point shall be below $0.1^\circ/\text{s}$ for each axis.

Table 3. Stabilisation phase performance requirements.

The control function for stabilisation of the coupled system shall be able to reduce the angular rates below 0.5 deg/s without exceeding the joint torque limits*.

* Repeated peak torque and momentary peak torque are respectively 176 Nm and 314 Nm.

Table 4. Safety requirements.

The distance between chaser and target surfaces shall not become smaller than 3 m as long as the rotational motion of Chaser and Target are not synchronised.

The distance between chaser platform and target surfaces shall not become smaller than 0.5 m during Synchronisation and Target Capture.

4. Control System Architecture

The GNC and Avionics architecture for COMRADE is illustrated in Fig. 3.

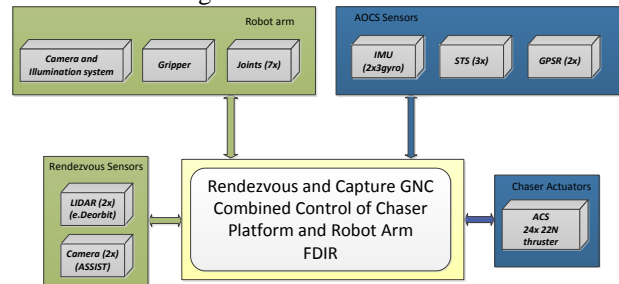


Fig. 3. COMRADE GNC and avionics architecture

The control architecture established for COMRADE covers both mission scenarios: ADR/e.Deorbit and ASSIST. The ADR/e.Deorbit scenario is more challenging in terms of relative navigation and agility requirements due to the uncooperative, tumbling target. Therefore the GNC and avionics architecture suitable for ADR/e.Deorbit is extendable to lower complexity ASSIST scenario.

The primary relative navigation sensor for the e.Deorbit scenario is a LIDAR which allows full relative pose estimation; whereas in the ASSIST scenario the target is equipped with markers which are tracked by a camera to derive a relative pose.

The robot arm and the actuators as well as the AOCS sensors (IMU, star tracker, GPS) are assumed to be the same for both scenarios. The actuation consist of 24x22 N thrusters for attitude and position control..

The robot arm is equipped with 7 joints, a gripper and a vision system for relative navigation between gripper and grasping point.

The combined controller for chaser platform and robot arm issues force and torque commands for the

platform, which are translated into thruster opening times by the thruster management function, and joint torque commands which are realised by the inner joint control loop. The inner joint control loop is closed by the joint torque sensors. It commands a motor torque to establish the desired joint torque level. The combined control loop also needs the joint position measurement as input.

Depending on the scenario and phase the control mode block and data flow vary from a common baseline— Fig. 4 is the diagram for the Reach phase.

During rendezvous and motion synchronisation the robot arm is not active. The feed-forward actions and state reference profile are computed by a dedicated guidance function. The navigation provides the current pose of the chaser relative to the target, including position, velocity, attitude and angular velocity. The control function of the chaser platform computes feed-forward and feedback control torques and forces, expressed in the chaser body frame, in order to follow forced motion trajectories in translation and attitude during the synchronization phase. It is a mode with fine pointing accuracy (compatible with sensor pointing performance and stability). It is robust to: High range of possible debris attitude motions; Navigation uncertainties in target attitude and relative state; Actuators misalignments/noises/delays; Fuel sloshing and flexible modes.

During the reach phase, the chaser performs station

keeping at the capture point while the robot arm moves the gripper towards the grasping point at the LAR of the target. This phase ends well before the first contact between gripper and grasping point is established. The navigation functions comprise the attitude navigation of the chaser platform in ECI frame as well as the relative (position and velocity) navigation between chaser and target and the visual servoing of the gripper w.r.t the grasping point. The combined control function issues force and torque commands for the chaser platform and joint torque commands for the robot arm. The force and torque commands are translated into thruster commands and then converted into realised forces and torques by the thruster model. The joint torque commands are translated into realised torques by the joint inner loop transfer function.

The control architecture in Capture phase, takes into account gripper sensors during capture. The control architecture is basically the same as the Reach phase. The only difference is the gripper control function which issues the gripper closure command as soon as the gripper is in the desired position and attitude for capture. The gripper was modelled as a single rigid body and contact dynamics is included in the simulations for this phase. The compliance controller implements a desired stiffness and damping for the end-effector, while keeping the chaser at the set point. The Capture Phase ends with the confirmation of the successful grasping by the gripper.

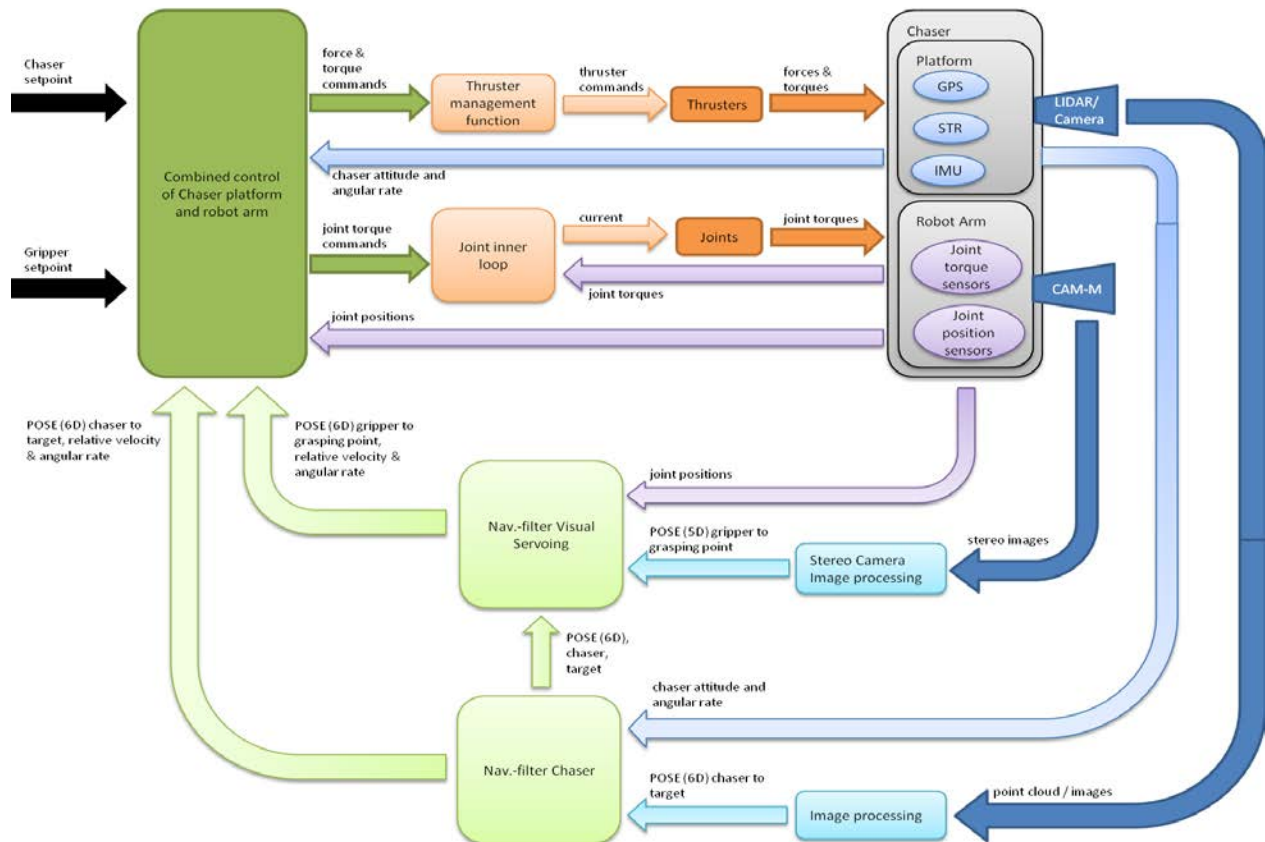


Fig. 4. Control Block Diagram for the Reach Phase

After capture the robot arm is rigidised. During this phase thruster commands are inhibited. Therefore only the robot arm control is active. The initial relative velocity between the chaser and the target has to be regulated to zero. Therefore, the joint angular rates are reduced until the brakes can be engaged. For this an appropriate impedance controller will be parameterized. In this controller, the joint torque limits of the arm will be considered. The navigation performance model is used for monitoring purpose during this phase.

At the end of the rigidisation the joint brakes are engaged. The stabilisation is performed employing the thrusters. The coupled system of chaser and target is detumbled by appropriate thruster commands. Constraints regarding the joint torque limits have to be respected. The control of coupled system is composed of two blocks, guidance and control. In this scenario, the control objective is to follow a decaying reference profile in terms of angular rate. In this phase, it is mandatory that the chaser remains synchronized with the target in order to reduce loads endured on the robotic arm's joints.

The Escape Mode with manipulator in closed loop consists of a trajectory planning part as well as a combined controller as the feed-back part. The trajectory planning needs information on the relative pose between the chaser and target, as well as the current robot joint positions, to compute a collision free escape trajectory.

The trajectory part of the Escape control module plans the trajectory such that the camera on the robot is pointing at the target, while avoiding collisions with the target, as well as self-collisions of the robot arm with the chaser. The Escape trajectory is computed such that it leads to a safe distance from the target.

The trajectory is planned for both the chaser as well as the robot arm. The combined feed-back controller of the Escape mode needs the chaser attitude, angular rate and relative position and velocity to the target, as well as the joint positions of the robot arm to accurately follow the computed Escape trajectory. The robust combined controller uses this sensor information to command force and torque commands to the chaser platform, as well as joint torque commands for the robot arm.

5. Nonlinear Simulator Design

The non-linear simulation environment allows accounting for effects that cannot be captured in linear analyses and evaluating performances in an environment that is closer to Real World.

This so-called Functional Engineering Simulator (FES) was developed in Matlab/Simulink R2017a and within the development framework GNCDE 3.9.0 [5],[6]. In addition, the referred framework contains a library (SPACELAB) with e.g. Sensors; Actuators; Dynamics, Kinematics, and Environment (DKE) models,

which have been utilised within the simulator instantiations. The implementation of the multi-body dynamics model has been carried out based on the Simscape Multibody technology.

The FES configuration for the different mission phases is as follows:

- Synchronisation: robot Arm is not moving and Chaser+Arm composite can be treated as a single rigid body (in order to improve CPU load for MonteCarlo campaigns). The Target position and attitude dynamics/kinematics are also computed independently.
- Capture: it lasts up to the contact between the gripper and the target grasping point. It implements the multi-body dynamics and kinematics (Simscape Multibody) for the Chaser/Arm chain and independently propagates Target position and attitude dynamics/kinematics.
- Composite: arm rigidisation and stack stabilisation. It implements the multi-body dynamics and kinematics model for Chaser/Arm/Target. Two different configurations are possible: free (Rigidisation phase) and locked flexible arm joints (Stabilisation phase). The robotic arm allows torque inputs to control the angle of each joint in free arm configuration. It also provides angular measurements of each joint.

The top-level architecture (Fig. 5) is common to all FES configurations, comprising the functional modules: Universe, DKE, Sensors, OBSW, and Actuators.

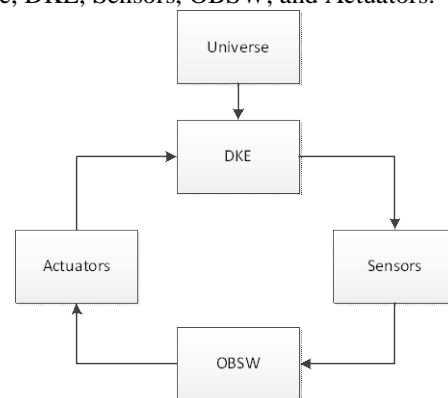


Fig. 5. FES top-level architecture.

The Universe module provides the DKE and Sensors with the ephemerides of Earth, Moon, and Sun.

The Environment module (within DKE) contains the environmental disturbances that may affect rotational and translational dynamics of the spacecraft. Both chaser and target will have each one an associated Environment module as some disturbances depend on specific spacecraft properties e.g. inertia matrix for gravity gradient torque. The list of disturbances modelled are:

- Central body acceleration

- Non-spherical gravity acceleration
- Gravity gradient torque
- Solar radiation pressure
- Third-body perturbation (Moon and Sun)
- Earth magnetic torque
- Aerodynamic drag

The Sensors module comprises all absolute sensors set:

- IMU (accelerometer and gyro)
- 3 Star Tracker heads
- Sun Sensor
- GPS receiver (and GPS constellation propagation)

The Actuators module is comprised of the RCS thrusters (24 in total).

6. Control Synthesis and Analysis

6.1 H_∞ Robust Control

6.1.1 Linear modelling approach

The H_∞ synthesis method adopted ([7],[8]) requires an LFT representation of the linearized flexible spacecraft model so that the plant model can consider parametric variations. An accurate and straightforward modelling technique of a multi-body system is the Two-Input Two-Output Port (TITOP) [9].

Fig. 6 depicts a sketch of a spacecraft model.

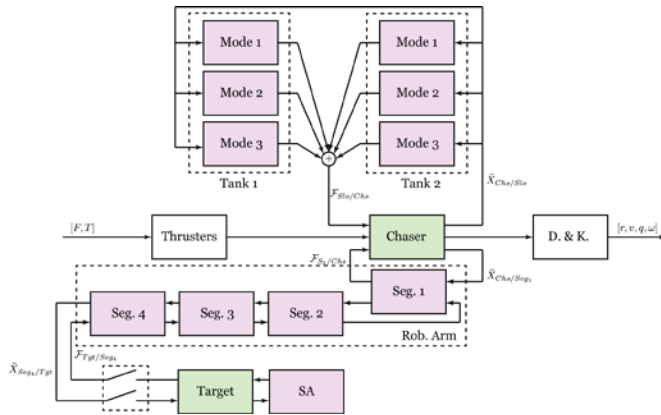


Fig. 6. Chaser-Target composite model based on TITOP models.

The chaser spacecraft is modelled as the hub TITOP which starts from its rigid dynamics, with uncertainty on mass and inertia parameters, and it is expanded to connect to two child elements: slosh modes, and the first segment of the capture arm. The thrusters block include thruster's misalignment with uncertainty and delay. The target is modelled with rigid body and solar array flexible modes. The switch illustrates that target and chaser may be physically connected.

6.1.2 Control Synthesis

The control synthesis methodology adopted is H_∞ Mixed Sensitivity Design [10]. The H_∞ control approach is added upon a nonlinear precompensation by computed torque control. Its synthesis process aims at shaping the sensitivity functions in order to achieve the closed-loop system performance and robustness requirements. Moreover, the sensitivity function shaping is achieved with frequency varying weights (of MIMO nature). The weight selection as well as the robust stability and performance analysis follows the process in [11], [12].

6.1.3 Synchronisation phase

The robust stability was analysed considering the closed-loop uncertainty system (81 states) with the synthesized controller. The resulting mu-analysis is shown in Fig. 8. Fig. 9 shows the robust performance mu-analysis results. Both analyses reveal full robustness within uncertainty set. In the analysis shown, frequencies are adaptively selected, and upper bounds are guaranteed to hold over each interval between frequencies.

6.1.4 Stabilisation phase

Robust stability and performance for stabilisation phase are shown respectively in Fig. 7 and Fig. 10. Robustness is ensured within uncertainty set.

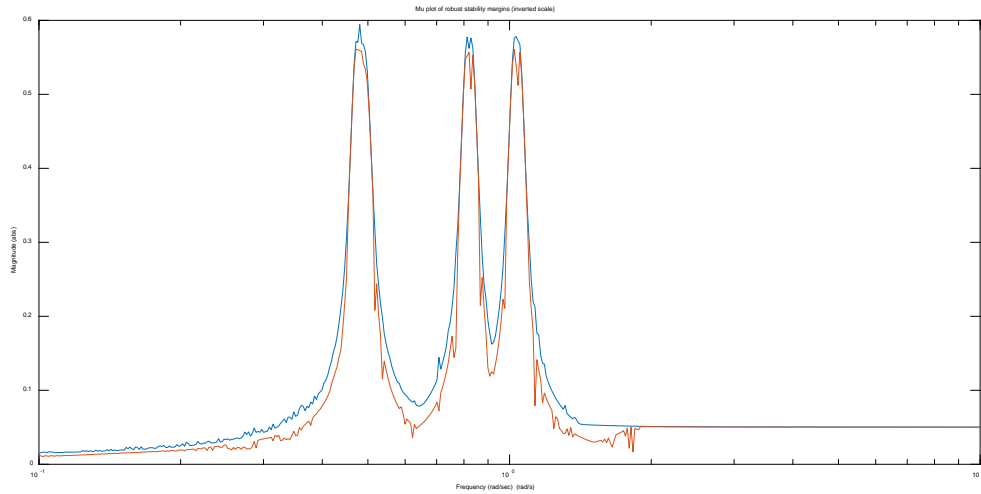


Fig. 8. Robust stability for synchronisation phase.

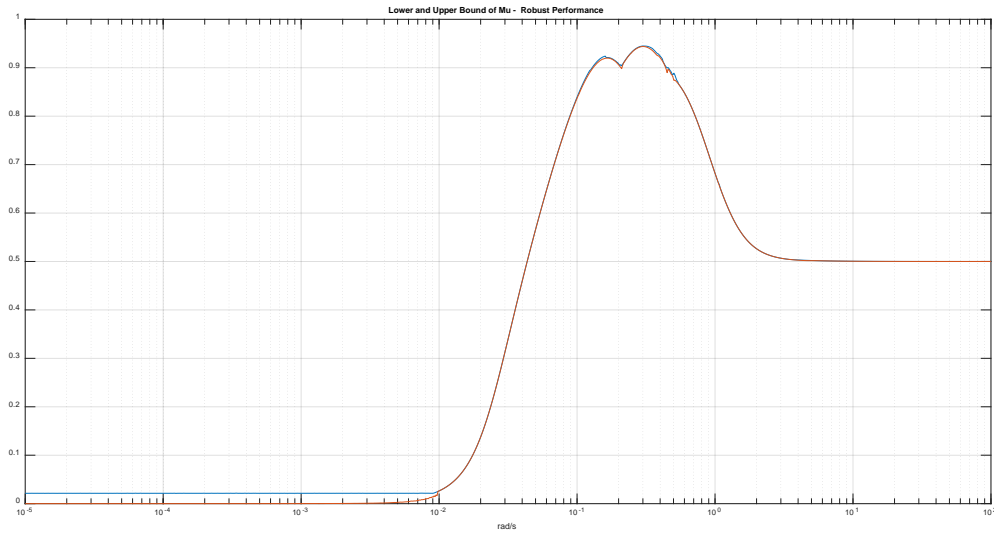


Fig. 9. Robust performance for synchronisation phase.

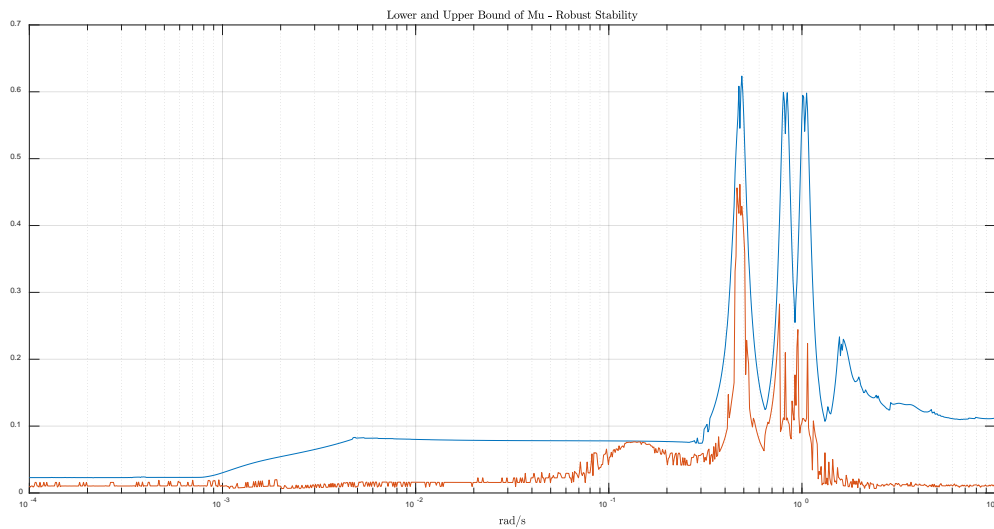


Fig. 7. Robust stability for stabilisation phase.

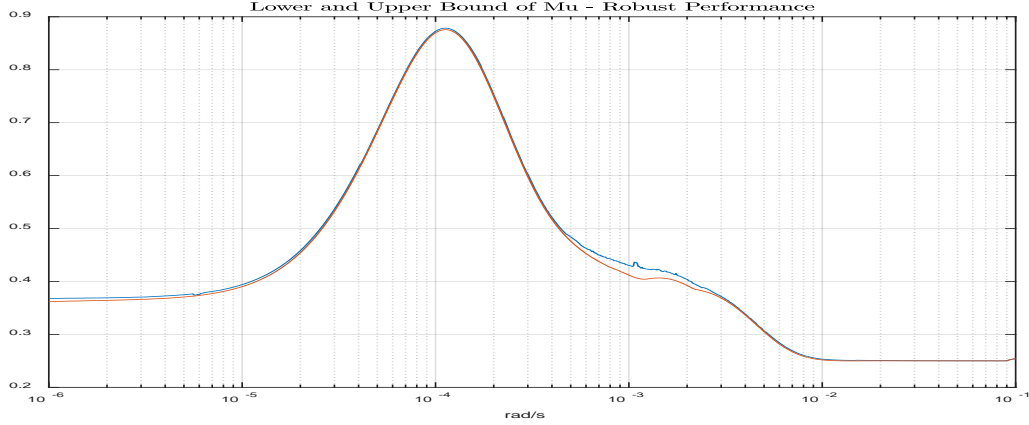


Fig. 10. Robust performance for stabilisation phase.

6.2 Nonlinear Compliance Control

6.2.1 Reach phase

The compliance controller used for capturing the target is designed with a nonlinear controller design technique using passivity argumentations. The controller design is motivated by a generalization of passivity based compliance controllers developed for fixed base [13] and floating base manipulators [14], [15], to the COMRADE case of a fully actuated compound satellite-manipulator system.

Fig. 4 shows the overall structure of the control loop during capture. As an external input a relative reference trajectory for the gripper $H_{te,des}(t), v_{te,des}(t)$ and the chaser setpoint $H_{tb,des}, v_{tb,des} = 0$ are given, that bring the gripper to the target frame and the chaser to a predefined configuration with respect to the target. The compound satellite-manipulator system is controlled by a 13 degrees of freedom controller that commands the generalized force to the chaser in a rate of 3Hz and the joint torques of the manipulator in a rate of 1kHz. As an input, the controller has access to the GNC sensors of the chaser, the joint sensors of the arm, as well as to the perception system that provides the 6D relative motion between the satellite and the target (based on LIDAR) in a rate of 3Hz, as well as the 6D relative motion between the gripper and the target (based on camera data) in a rate of 10Hz.

The controller aims at a convergence of the chaser and end-effector frames relative to the target, i.e. H_{te}, H_{tb} , to the desired poses $H_{te,des}(t), H_{tb,des}$.

The controller is designed by aiming at a closed loop structure as the one resulting from PD+ control [16] in case of fixed base manipulators.

If the control algorithm described above is directly implemented based on the measurements from the LIDAR and the camera, as shown in Fig. 11, the overall control loop is affected by the sampling rates of the perception system, i.e. 10Hz for measuring H_{te} via the

cameras and 3Hz for measuring H_{tb} via the LIDAR. Therefore, any increase in these sampling rates, e.g. increasing the GNC control from 3Hz to 10Hz, might be advantageous for the overall control performance. In the COMRADE project we also investigate an alternative control structure as depicted in Fig. 12, in which the basic feedback controller is computed using its joint data which is available with a fast 1kHz sampling.

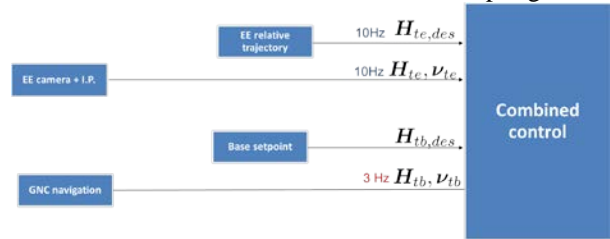


Fig. 11. Combined controller with navigation and camera signals.

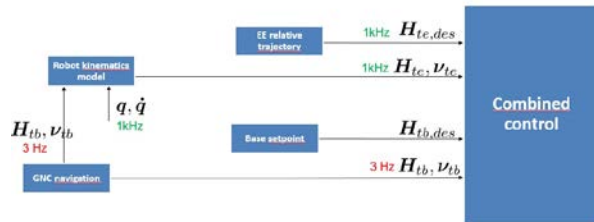


Fig. 12. Alternative scheme relying only on navigation.

The combined controller leads to a closed loop structure similar as the PD+ tracking control for fixed base manipulators [16]. The stability analysis of this controller is based on a continuous-time analysis using the full nonlinear dynamics, i.e. no linearization or other approximation is required. A strict Lyapunov function for the PD+ control is given in [17], proving asymptotic stability. It should be noted that the stability in the nominal case (i.e. without delay and with continuous control) is guaranteed for arbitrary positive definite

gains. The same analysis applies also to the present case.

The extension to the redundant case is treated in [13][20]. In order to consider the effects of the time discretization of the controller the used gains were designed based on the bandwidth of the linearized system.

6.2.2 Rigidisation phase

The controller of the arm for the rigidisation phase focuses on the damping of the remaining relative velocity. The control structure of the compliance controller as a basis is used but choosing a parameterization that implements mainly the damping control with a proportional term, which allows bringing the arm back into the grasping configuration.

The design of the rigidisation torque-based control has to fulfil two main points:

1. Joint velocities have to decrease to zero in a stable manner,
2. The commanded torque signals should not exceed the actuator maximum torque.

The first condition can be achieved by using a proportional-derivative control architecture. This structure is referred as the PD control law. Usually this scheme is designed disregarding the inherent power supply limitation of the joint actuators. Such limitation has a saturation effect in the signal transfer from the controller's output to the manipulator input.

Therefore a PD-controller with a linear saturation does not ensure globally the achievement of the regulation objective and it might lead to undesirable effect in the closed-loop system.

The design of the control law for the rigidisation phase has the following expression:

$$u = -s(K_d \dot{q} + K_p \bar{q}) = s(\tau)$$

where $\bar{q} = q - q_d$ is the error between the measured joint position q and the desired position q_d being the one at the capture point. The joint velocity is \dot{q} and K_p , K_d are positive definite diagonal matrices. The components in parenthesis represent the classical PD control at joint level. Furthermore, the function $s(\tau)$ has been introduced as a meaning of saturation function due to the limitation of the actuator to apply a maximum torque. Stability of PD control with bounded input has been proved by [19]. It consists of a special form of the natural saturation and the stability is proved under the condition that the saturation function for the PD torque controller must be a *strictly increasing linear saturation function*. Therefore, the function s has been designed to be strictly increasing in order to exploit the stability proof described in [19]. Given a constant M , a function s is said to be a *generalized saturation* with bound M , if

it is locally Lipschitz, non-decreasing and satisfies the following:

- $\tau s(\tau) > 0$ for all $\tau \neq 0$
- $|s(\tau)| \leq M$ for all $\tau \in \mathbb{R}$.

And given positive constant L with $L \leq M$, a function s is said to be a *linear saturation for (L,M)* if it is locally Lipschitz, non-decreasing and satisfies the following.

- $s(\tau) = \tau$ when $|\tau| \leq L$
- $|s(\tau)| < M$ for all $\tau \in \mathbb{R}$.

Therefore, it allows to define the saturation function for each i -th torque-component as follows:

$$s(\tau_i) = \begin{cases} -L_i + (M_i - L_i) \tanh\left(\frac{\tau_i + L_i}{M_i - L_i}\right) & \text{if } \tau_i < -L_i, \\ \tau_i & \text{if } |\tau_i| \leq L_i, \\ L_i + (M_i - L_i) \tanh\left(\frac{\tau_i - L_i}{M_i - L_i}\right) & \text{if } \tau_i > L_i. \end{cases}$$

Where M_i is the torque-limit that the i -th actuator can supply.

Fig. 13 shows a comparison between the designed saturation function and a classical linear saturation for a given input torque, τ .

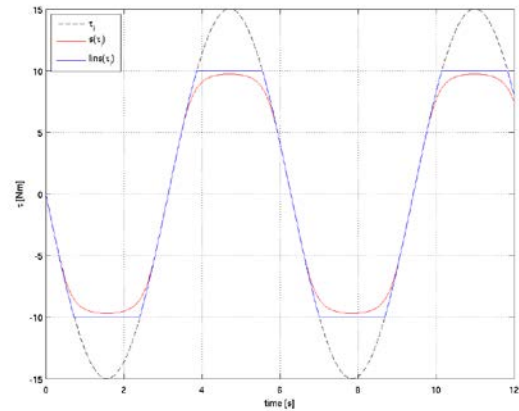


Fig. 13. Comparison between designed saturation (red line), linear saturation (blue line) for the torque input (dashed line).

6.3 Health Monitoring System

Both the force/moment direction and the fault compensability analysis demonstrate that there exists an important degree of redundancy in the thruster set. This fact leads a constrained force/moment allocation algorithm scheduled by a robust FDI scheme, to be probably the most appropriate solution to solve the FDA problem. Thus, it is proposed in the following to develop such a solution. The H_∞ Unknown Input Observer (UIO) strategy with the Nonlinear Inverse Pseudo Controller technique (NIPC) are proposed for that purpose.

As it has been already stated in [21],[22], thruster faults affect in a more severe manner the rotational dynamics than the translational ones. Furthermore, it has been shown in these papers that the Euler's angle (or quaternion) measurement is not necessary. A direct consequence is that the model used for the design of the FDI unit, is the one that links the actuator (thruster) commands with the rotational measurements (rotational velocities).

The rotational motion of the chaser caused by an applied moment (sum of all torques acting on it) can be derived from the Euler's second law in the so-called body frame. The endogenous torque $T_s \in \mathbb{R}^3$ is assumed to be mainly due to propellant sloshing in the two tanks. It is modelled in this work as a 3D spring-mass model. Thus, the moment is deduced from a mass-spring damper vector-based equation. The analysis of this model demonstrates that only the dominant sloshing mode has a real impact on the rotational velocities. Thus, it is proposed to derive from the main equation a reduced order model with the objective to capture the main dynamics. For this purpose, a state space model of order 8 was proposed, which preserves the fundamental Euler's second principle.

With regards to the possible faults occurring in the thruster-based propulsion system, the focus is on the "stuck-open" and "stuck-closed" faults type. Such faults can be modelled in a multiplicative manner as can be seen in [21],[22].

From the fault diagnosticability and compensability analysis presented in the note "Drafting the faulty scenarios for thrusters and joints", it is proposed to focus on thrusters N°. 1,5,13 and 17 since they correspond to the most difficult problem in terms of FDA task.

To solve the FDI problem, the proposed solution consists of a bank of 4 dedicated H_∞ UIOs, designed according to the following strategy: The first H_∞ UIO is designed so that the estimation error behaves in the orthogonal space of the plane induced by the moment directions of the thruster 1; The three other H_∞ UIOs follow the same principle for the thruster 5,13,17.

Thus, the UIO with the minimum estimation error (in the sense of the 2-norm) indicates that a fault occurs in the associated thruster.

Once a faulty thruster has been diagnosed by the UIO-based FDI unit, a fault accommodation mechanism has to be engaged in order to maintain the capture objectives. As explained in the preliminaries, the configuration of the thrusters disposes a lot of degrees of freedom. Particularly, the set of $N=24$ thrusters is placed on the chaser spacecraft such that the nominally attainable set of propulsion moments and forces is relatively close to the sets obtained by combining the thrust of any $N-1=23$ thrusters. From a practical viewpoint it means that it is possible to achieve the

required control performance with only 23 healthy thrusters. This motivates to propose the fault tolerance solution to be based on control allocation philosophy. Thus, as soon as the i th thruster is confirmed to be faulty by the UIO-based FDI scheme, the desired forces and torques are redistributed among the remaining $N-1$ healthy thrusters. The original version of the NPC algorithm was presented by [23] and further developed for fault tolerance purpose in [24]. The core of the fault tolerance principle is that if the i th thruster is faulty, then the i th component of u_{max} is set to 0. The weighting matrix W affects the prioritization among torque/force components when $Mu_{THR} - v$ cannot be attained due to thruster physical constraints. The different choices of the vector p -norm in result in: Minimum flow rate allocation: $p=1$; Minimum power allocation: $p=2$; Minimum peak torque/force allocation: $p=\infty$.

From good surveys about model-based FTC solutions (see for instance see [25], [26], [27], [28], [29]), following limitation on existing approaches can be identified: the FDI solution is developed independently from the FTC solution. Thus, there is no guarantee of global optimality of the overall solution. This problem is addressed in the COMRADE project using the concept of supervisory FDA with mutual performance optimization [30]. This is thought "a new way to think about the FDA problem" since, it is tolerated to have a non-perfect FDI scheme in the sense that it is tolerated to have false alarms and missed detection, thanks to the global optimality of the FDA scheme which guarantees that fault tolerance is always maintained. The price to pay results in the transient behaviour of the system since a chattering phenomenon of the control signal, may occur. If the chattering duration is maintained during an important time, then the transient performance cannot be guaranteed. Fortunately, the proposed method is able to minimise this time since the criteria that is proposed to minimize (the so called *dwell-time*) is related to it.

The structure of the problem, also called the supervisory FDA architecture that is proposed to solve this problem is as shown in Fig. 14.

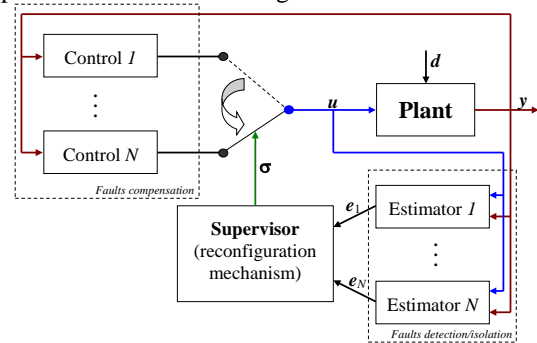


Fig. 14: The structure scheme of the supervisory FTC system

The supervisor has to ensure right continuity of the signal $\sigma(t)$, i.e. the signal has to be piecewise continuous and between any two jumps a time delay should exist. The design of the map differs depending on operation conditions and the blocks' properties. Then, there exists a converging estimator that solves the mode estimation problem. As it is well known, the optimality of the subsystems does not imply the same property for the whole system. In the proposed method the optimal properties are critically dependent on switching and, hence, on the supervisor.

The main advantage of the method proposed by IMS lab. is concerned by an approach to the system design oriented on the mutual performance optimization of this switched system. For this purpose, the method chooses a characteristic of the hybrid system to be optimized in parallel with the conventional ones used for the multi-estimator and the control design. The criterion to be minimized is the minimal admissible time between switches among controls (the minimum delay between switches is called *dwell-time*). It is well known that switching among stable linear systems does not lead to instability if the delay between switches are big enough. This is why the strategy oriented on this delay increasing is frequently applied in practice to ensure stability in switched systems. However, for FTC problems, such an approach is not admissible, since it results in an increasing time of reconfiguration time. Additionally, it may lead to a longer period of wrong control activation for the faulty plant. The both properties are inadmissible from a practical point of view. IMS lab. Has established stability theorems and corollaries for both constant and time varying plant index $i \in I$, see [30].

The dwell-time supervisory-based FDA solution has been very recently extended by IMS. Lab, to the virtual actuator paradigm. The goal we pursue is to select timely the suitable FTC controller from a bank of virtual actuators. Fig. 15 illustrates the supervisory-based virtual actuator scheme. As it can be seen in this figure, the input of the nominal control law is given by $y + Cx_{v_k}$ where x_{v_k} corresponds to the state of the selected virtual actuator.

Thus, by virtue of the dwell-time theory, it can be proven that the proposed supervisory FDA scheme is exponentially stable. The proof is not given there for brevity.

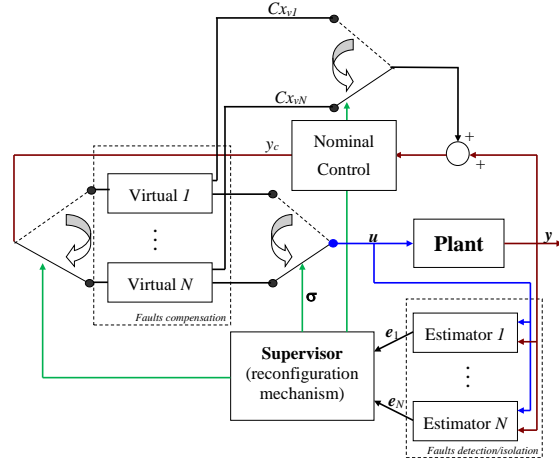


Fig. 15.: The structure scheme of the supervisory-based virtual actuator

Following the methodology presented in the above section and since we are focusing on stuck-open and stuck-closed fault types for thrusters N^o. 1,5,13 and 17, we have a total of $N=9$ functioning modes, i.e. 8 faulty modes and the nominal one. Thus, the multi-estimator consists of a total of 9 estimators. Then the problem turns out to be the design of the estimator gains $L_i, i = \overline{1,9}$. These gains are designed so that the estimation errors $e_i, i = \overline{1,9}$ for the matched cases are robust to the disturbance torque T_d , in the H_∞ -norm sense. To proceed, the technique considers that the disturbance torque T_d has frequency spectrum which can be approximated by linear dynamics with input vector d .

The robust performance analysis of the FDI scheme shows that: the considered uncertainties do not affect the transfer $T_{T_d e}(s)$ which is quite reassuring since they are mainly concerned by the actuation unit; with a gain at low frequencies between -15dB and -30dB, the estimation performance will be affected by the uncertainties. This is not a important problem since, as explained previously, *i*) this problem can be managed through the hysteresis parameter of the dwell-time supervisor and, *ii*) the philosophy of the supervisory-based FDI scheme is that a false alarm is completely tolerated, thanks to the global optimal stability proof.

7. Nonlinear Simulation Results

The model-in-the-loop test campaign plan is summarised next. Then the respective simulation results compared and used for comparison of both H_∞ robust control and nonlinear compliant control approaches.

7.1 MIL Test Plan

The model in the loop test plan for the edeorbit case considers three different target rotational states as baseline scenarios, considering 2.5 deg/s angular velocity.

Scenario 1

- Spin axis in body frame is aligned with the +Ys axis.
- Spin axis in LVLH frame is aligned with the +H-bar axis.

Scenario 2

- Spin axis in body frame is along a direction contained in the YsZs plane at 45 degrees w.r.t. +Ys and +Zs.
- Spin axis in LVLH frame is aligned with the +H-bar axis.

Scenario 3

- Spin axis in body frame is aligned with the +Zs axis.
- Spin axis in LVLH frame is at an angle of 45 degrees with respect to the +H-bar axis and is contained in the H-bar/R-bar plane.

On the other hand the ASSIST case is expected to be less GNC demanding as the target is cooperative i.e., null relative angular velocity. For simplification and contrasting with the edeorbit case, the target is assumed a 2x2x2m cube, 1800kg mass and [7000 2500 6500]kg.m² moments of inertia.

7.2 Control Systems Validation

GNC performance errors are used for metrics for controller comparison. Safety requirements (Table 4) are ensured by design of guidance law, although chaser-target structural distance was monitored in simulations.

Platform actuation has been kept away from saturations in synchronisation and capture phases. Robot arm loads were verified to be within permissible range for rigidisation and stabilisation phases.

Table 5 highlights the achieved chaser platform performances (mean value of 100 simulations) during Monte Carlo test campaign for synchronisation and reach phases.

For synchronisation phase only H_∞ robust control was developed. The performance specifications for this phase are in Table 1. The errors are mostly within specification. The only statistic borderline outside is pointing accuracy, when accounting for standard deviation, which should be $< 2^\circ$.

Table 5. Chaser platform performance (capture point).

	Synch. phase	Reach phase	
	H_∞	H_∞	Nonlinear Compliant
Position [m]	0.067±	0.023±	0.026±
	0.028	0.008	0.011
Velocity [m]	0.006±	0.002±	0.001±
	0.002	<0.001	<0.001
Pointing [deg]	1.544±	0.318±	0.105±
	0.619	0.153	0.077
Angular rate [deg/s]	0.155±	0.075±	0.114±
	0.089	0.041	0.047

For reach phase both H_∞ robust control and nonlinear compliant control are simulated. The applicable performance specification is in Table 2. All errors are well within requirements. In terms of relative position tracking both controllers behave similarly. The nonlinear compliant controller has tighter tracking in pointing accuracy.

Table 6 presents the end-effector performance relative to the grappling point in the target. Again, applicable requirements are in Table 2.

Regarding position and pointing accuracy both controllers are within the requirements.

The velocity and angular rate do not fulfil the requirements neither for the H_∞ robust controller nor for the nonlinear compliant control considering the maximum values achieved during the Monte Carlo test campaign.

Regarding velocity and angular rate, achieved Monte Carlo test campaign mean value are better for the H_∞ control. For the compliance control, the performance is borderline outside the velocity requirement (<0.005m/s), and outside for angular rate (0.1°/s).

Note that, during the H_∞ control simulation test cases, it has been observed that a very gentle contact can lead (when contact extends over long periods) to a rather reactive behaviour of the gripper resulting in peaks for position, attitude, velocity, and angular rates that do not always settle till the end of the simulation. These runs were removed from the statistics as outliers since the initial impulse that starts the motion is not representative of the underlying physics to be modelled (it is the result of numerical stiffness in the contact dynamics modelled in Simscape Multibody model). For compliance control, it has been usually possible to achieve a stable and successful grasp in presence of contact.

Table 6. Gripper performance mean values (reach)

		H_∞	Nonlinear Compliant
Position [m]	X	-0.001±0.004	0.004±0.003
	Y	0.002±0.005	0.005±0.003
	Z	-0.001±0.004	0.003±0.002
Velocity [m]	X	0.001±0.003	0.004±0.003
	Y	0.001±0.003	0.005±0.003
	Z	-0.001±0.002	0.005±0.003
Pointing [deg]	X	-0.016±0.105	0.120±0.084
	Y	-0.033±0.140	0.086±0.054
	Z	-0.015±0.293	0.182±0.113
Angular rate [deg/s]	X	0.011±0.073	0.520±0.335
	Y	-0.004±0.098	0.286±0.217
	Z	0.029±0.191	0.434±0.314

For the rigidisation phase closure of the gripper has already been executed and the chaser is effectively connected to the target. Platform control is disabled and robot arm joint rates are dampen before engaging the joint brakes. Table 7 collects both position and velocity errors for the joint states. Specific requirements are not available for this operation. For joint velocity, the error achieved for the H_∞ robust controller is 21%, of the one for the compliant controller case. However, the nonlinear compliant control respects the torque limits around the actuation z-axis even considering initial velocity of the joints, which makes the control action more challenging.

The achieved joint position error for the H_∞ robust controller is 60% of the one for the compliant controller case. The team is confident that better joint position performances for the nonlinear compliant control can be achieved (future work) by a more adjusted tuning of the position gains in case a specific requirement for the joint positions is given.

Table 7. Joint-immobilisation performance (rigidisation)

	H_∞	Nonlinear Compliant
Angle [deg]	1.618±0.809	2.710±1.169
Angular rate [deg/s]	0.016±0.013	0.078±0.030
Initial angular velocity [deg/s]	0.14±0.20(1 σ) (Max=3.02)	(1,1,1,1,1,1)
Maximum torques around the actuation axis (z) for all the 7 joints [Nm]	(3.87, 12.23, 3.42, 29.80, 12.28, 8.11, 28.10)	(10.94, 12.89, 19.83, 50.10, 17.16, 23.32, 41,45)
Simulation time[s]	120 s	120 s

At last, the stabilisation phase comprises the de-tumbling of ENVISAT. The requirement for this operation is in Table 3. Table 8 confirms the requirement is comfortably met.

Table 8. ENVISAT de-tumbling performance (stabilisation phase).

		H_∞
Angular rate [deg/s]	X	-0.023
	Y	0.006
	Z	0.013

8. Conclusions

COMRADE project has currently finalized the Model-in-the-Loop (MIL) level validation phase with successful results and will now enter into the Processor-in-the-Loop (PIL) and HW-in-the-Loop (HIL) validation level to verify that the designed algorithms are robust to modelling uncertainties with respect to space-representative avionics and real HW (sensors).

The main conclusions that can be derived from the MIL-based design/validation phase are:

- Full Control System design for an in-orbit servicing scenario has been performed, covering approach and synchronization phase, reach/capture/rigidization phase and stabilization/detumbling phase.
- The Control System has included Guidance, Navigation, Controller, FDA/FTC and Modes Manager functions, with special emphasis on Controller function design, analysis and validation.
- The in-orbit servicing scenario has considered two significantly different missions: an Active Debris Removal mission with uncooperative ENVISAT satellite as target, and re-fuelling mission with a cooperative GEO satellite target.
- For the two missions, a common Control System architecture and implementation has been proposed, developed and demonstrated.
 - Modularity has been a must for finding the common architecture.
 - Easy re-tuning process of the system has been a must for applying the same algorithms to both missions.
- Approach/synchronization phase has considered robust H_∞ 6DOF controller over a rigid body with sloshing and flexibility (solar arrays, stored robotic manipulator) effects as main perturbations. The linear (μ -analysis) and non-linear (Monte Carlo with non-linear MIL simulator) results have demonstrated the

required performances (including robust performance and stability).

- Reach, capture and rigidization phase has considered a dual approach and implementation:
 - Robust H_∞ 13DOF controller over a multi-body system composed by the spacecraft platform plus a robotic manipulator with 7DOF (and grasping/re-fuelling end-effect at the end).
 - A compliance/impedance 13DOF controller over the same multi-body system as for the robust H_∞ controller.

Both controllers have demonstrated to be valid options with some better performance results obtained for the first one during this activity. The second controller type had some more difficulties to meet some of the requirements and some additional work is still needed in the future. On the other hand, it has been easier to apply the second controller over existing contact dynamic models than the first one, which can be an indication for future work for specific phases involving contact between two bodies.

- Stabilization/detumbling phase has considered robust H_∞ 3DOF attitude controller over the full composite (chaser spacecraft + target spacecraft + rigidized robotic manipulator joining both vehicles) with sloshing and flexibility (solar arrays, stored robotic manipulator) effects as main perturbations. Obtained results have demonstrated the required performances (including robust performance and stability).
- Advanced FDA/FTC techniques have been also considered as an additional Failure Detection and Accommodation layer on top of the nominal control design. The design of such layer has been presented while implementation and results will be available only during next phase of COMRADE.

References

- [1] Satellite Collision Leaves Significant Debris Clouds. NASA Orbital Debris Quarterly News. Volume 13, Issue 2. April 2009
- [2] Space sustainability. Adoption of Notice of ISO 24113: Space systems – Space debris mitigation requirements, ESA ECSS-U-AS-10. 10.02.2012.
- [3] e.Deorbit Consolidation Phase Mission and System Requirement Document (MSRD). Iss. 1, Rev. 0. 20.04.2017
- [4] Statement of Work for the hARmonised System Study on Interfaces and Standardisation of fuel Transfer (ASSIST). TEC-MMA/2014/133. ITT/1-7968/14/NL/SFe. Issue 1.0. 13/06/2014
- [5] F. Gandía et. al., “GNCDE: an integrated GNC development environment for attitude and orbit control systems”, ICATT 2012
- [6] L. Strippoli et al., “GNCDE as DD&VV Environment for ADR Missions GNC”, 6th ICATT. Darmstadt, 2016
- [7] Doyle, J.C., K. Glover, P.P. Khargonekar, B.A. Francis, “State-space solutions to standards H2 and Hinf control problems”, IEEE Transactions on Automatic Control, vol. AC-34, no. 8, pp. 831-847, 1989.
- [8] Doyle, J.C., “Robust and optimal control”, Proceedings of the 35th Conference on Decision and Control, Kobe, Japan, Conference Proceedings, pp. 1595 – 1598, 1996.
- [9] D. Alazard, J.P. Gonzalez, T. Loquen, C. Cumer, “Two-input two-output port model for mechanical systems”, AIAA, 2015, pp. 203–210.
- [10] F. Ankersen, “Guidance, Navigation, Control and Relative Dynamics for Spacecraft Proximity Manoeuvres”, PhD Thesis, 2010.
- [11] T.V. Peters, N.M.G. Paulino, F. Gandía, “Investigation of Active Detumbling Solutions for Debris Removal”, Clean Space Industrial Days, ESA/ESTEC, Netherlands, 2016, 23-27 May.
- [12] J.F. Vasconcelos et al., “GNC design and validation for rendezvous, detumbling, and de-orbiting of ENVISAT using a clamping mechanism”, 6th International Conference on Astrodynamics Tools and Techniques, Darmstadt, Germany, March 2016
- [13] Ch. Ott, “Cartesian Impedance Control of Redundant and Flexible-Joint Robots”, Springer Tracts in Advanced Robotics (STAR), Vol. 49, Springer-Verlag, 2008.
- [14] A. M. Giordano, G. Garofalo, M. De Stefano, Ch. Ott, A. Albu-Schäffer, “Dynamics and control of a free-floating space robot in presence of nonzero linear and angular momenta”, IEEE Annual Conference on Decision and Control (CDC), 2016.
- [15] M. De Stefano, J. Artigas, A. M. Giordano, R. Lampariello, A. Albu-Schaeffer, “On-ground experimental verification of a torque controlled free-floating robot”. 13th Symposium on Advanced Space Technologies in Robotics and Automation (ASTRA 2015), ESA/ESTEC, Noordwijk, the Netherlands, 11-13 May 2015.
- [16] B. Paden, R. Panja, “Globally asymptotically stable 'PD+' controller for robot manipulators”, International Journal of Control, 47, pp. 1697-1712, 1988.
- [17] V. Santibanez, R. Kelly, “Strict Lyapunov Functions for Control of Robot Manipulators”, Automatica, 33, pp. 675-682, 1997.
- [18] M. De Stefano, R. Balachandran, A. M. Giordano, C. Secchi, “An Energy-based Approach for the

- Multi-Rate Control of a Manipulator on an Actuated base”, IEEE International Conference on Robotics and Automation, Brisbane, Australia, 21-25 May, pp 1072-1077, 2018
- [19] A. Zavala-Rio and V. Santibanez, "Simple extensions of the PD-with-gravity-compensation control law for robot manipulators with bounded inputs," in IEEE Transactions on Control Systems Technology, vol. 14, no. 5, pp. 958-965, 2006.
- [20] Ch. Ott, A. Kugi, and Y. Nakamura, "Resolving the Problem of Non-integrability of Nullspace Velocities for Compliance Control of Redundant Manipulators by using Semi-definite Lyapunov functions". IEEE International Conference on Robotics and Automation, pp. 1999-2004.
- [21] D. Henry. Fault Diagnosis of the Microscope Satellite Thrusters using Hinf/H- Filters. AIAA Journal of Guidance, Control, and Dynamics. vol 31, n. 3, pp. 699-711.
- [22] R. Fonod, D. Henry, C. Charbonnel and E. Bornschlegl. "Position and Attitude Model-Based Thruster Fault Diagnosis: A Comparison Study". AIAA Journal of Guidance, Control, and Dynamics. vol. 38. N°6. pp. 1012-1026.
- [23] Jin, H. P., Wiktor, P., & DeBra, D. "An optimal thruster configuration design and evaluation for quick step". Control Engineering Practice, 3, 1113–1118.
- [24] R. Fonod, D. Henry, C. Charbonnel, E. Bornschlegl, D. Losa, S. Bennani. "Robust FDI for fault-tolerant thrust allocation with application to spacecraft rendezvous". Control Engineering Practice. vol. 42. pp. 12-27.
- [25] "Fault-tolerant control systems: The 1997 situation". In IFAC SAFE-PROCESS'97, volume 3, pages 1033-1054, Kingston Upon Hull, United Kingdom
- [26] Aström K., Albertos P., Blanke M., Isidori A., Schaufelberger W., Sanz R. "Control of Complex Systems". Springer Verlag.
- [27] Blanke M., Kinnaert M., Lunze M., Staroswiecki M. "Diagnosis and fault tolerant control". Springer, New York
- [28] Henry D. "From fault diagnosis to recovery actions for aeronautic and aerospace missions: A model-based point of view". Plenary session in the 23rd IAR Workshop on Advanced Control and Diagnosis. Coventry, UK, pp. 13–19
- [29] Zhang Y., Jiang J. "Bibliographical review on reconfigurable fault-tolerant control systems." Ann. Reviews in Control, 32(2), pp. 229–252.
- [30] D. Efimov, J. Cieslak and D. Henry. "Supervisory Fault Tolerant Control with Mutual Performance Optimization". International Journal of Adaptive Control and Signal Processing, vol. 27 (4), pp. 251–279